2018

Numerical and Experimental Study of Flapping Foils with Dynamic Wall Effect

Jeong-Yong Park
University of Rhode Island, jeongyong_park@my.uri.edu

NUMERICAL AND EXPERIMENTAL STUDY OF FLAPPING FOILS WITH DYNAMIC WALL EFFECT

BY

JEONG-YONG PARK

A THESIS SUBMITTED IN PARTIAL FULFILLMENT OF THE

REQUIREMENTS FOR THE DEGREE OF

MASTER OF SCIENCE

IN

OCEAN ENGINEERING

UNIVERSITY OF RHODE ISLAND

2018

MASTER OF SCIENCE THESIS

OF

JEONG-YONG PARK

APPROVED:

Thesis Committee:

Major Professor Jason Dahl

Stephen Licht

Isaac Ginis

Nasser H. Zawia

DEAN OF THE GRADUATE SCHOOL

UNIVERSITY OF RHODE ISLAND

2018

ABSTRACT

The existence of a wall near a foil body in a freestream influences the hydrodynamic forces exerted on the body. In this research, numerical simulations are performed to investigate the hydrodynamics of a NACA 0012 foil with wall effects using open source software, a 2-D Navier-Stokes solver based on the Boundary Data Immersion Method (BDIM). The inherent difference between the 2-D and 3-D dynamic wall effects is shown by comparing experimentally obtained measurements of vortex shedding behind a flapping foil with a numerical simulation using the same kinematics. The differences are significant in terms of the thrust force coefficient profiles and the vortex development. Particle image velocimetry (PIV), using data from an experiment, shows that the vortex at the tip significantly influences the formation and phasing of the wake.

ACKNOWLEDGMENTS

I first acknowledge Dr. Jason Dahl, for helping me with this research and international student life in the United States. Thanks also to my great coworkers and colleagues: Amin, Deniz, Erdem, Jack, Letti, and Stephanie. Finally, thanks to my wife, Seulah, for her infinite faith and love. You all really encouraged me every minute to complete my graduate program. Thank you all very much.

PREFACE

This thesis is formatted in accordance with the guidelines for a manuscript typed thesis. The manuscript is prepared to be submitted to Bioinspiration & Biomimetics. All work in the manuscripts was done by the authors listed.

TABLE OF CONTENTS

Page

LIST OF FIGURES

LIST OF TABLES

MANUSCRIPT 1

Numerical and Experimental Study of Flapping Foils with Dynamic Wall Effect

by

Jeong-Yong Park[1], Jason M. Dahl[1], Stephanie Steele[1], Alexander Stott[1], Amin Mivehchi[1], Stephen Licht[1]

[1] *Department of Ocean Engineering, University of Rhode Island, United States*

Prepared to publish in Bioinspiration & Biomimetics

1.1 Abstract

The existence of a wall near a foil body in a freestream influences the hydrodynamic forces exerted on the body. In this research, numerical simulations are performed to investigate the hydrodynamics of a NACA 0012 foil with wall effects using open source software, a 2-D Navier-Stokes solver based on the Boundary Data Immersion Method (BDIM). The inherent difference between the 2-D and 3-D dynamic wall effects is shown by comparing experimentally obtained measurements of vortex shedding behind a flapping foil with a numerical simulation using the same kinematics. The differences are significant in terms of the thrust force coefficient profiles and the vortex development. Particle image velocimetry (PIV), using data from an experiment, shows that the vortex at the tip significantly influences the formation and phasing of the wake.

1.2 Introduction

Ground effect produces a significant change in force exerted a lifting surface compared with the freestream. This can be seen in operation when in close proximity to the ground (Cui and Zhang, 2010). This phenomenon has been researched extensively, especially in aerodynamics, since it can contribute to lift efficiency. In contrast with static ground effect, the airfoil lift and circulation around the foil becomes time variant in dynamic ground effect and the behavior generates an unsteady fluid wake around the foil (Chen and Schweikhard, 1985). This paper investigates the difference between 2-D and 3-D wall effects of heaving and pitching foils through numerical simulation. We call it the 2-D dynamic wall effect when it occurs with a lifting surface that has an infinite span or high aspect ratio.

In previous 2-D numerical studies, similar foil motions were used with various methods for different applications, such as thrust propulsion of underwater

vehicles or micro aerial vehicles (Karbasian and Esfahani, 2017; Wu et al., 2014b; Moriche et al., 2015; Wang and Yeung, 2016) and power extraction from tidal currents (Wu et al., 2014a; De Silva and Yamaguchi, 2012). Molina and Zhang (2011) examined the downforce of a race car spoiler with oscillating heave motion using Reynolds-average Navier-Stoke solver and showed three different regimes in the flow. At low reduced frequency, the ground effect dictates the flow, and the airfoil can be assumed in a quasi-stationary motion. Meanwhile, at medium frequencies, an incidence effect occurs along the effective angle of attack, and at high frequencies, there is a prominent added mass effect. Liang et al. (2014) used a discrete vortex potential flow method with only a heaving motion of NACA 0012 over a plane surface. The time-averaged lift coefficient increases swiftly as the gap ratio decreases. It was also demonstrated that a higher reduced frequency produces larger amplitudes of the lift coefficient. However, the reduced frequency does not have a noteworthy influence on the time-averaged lift coefficient. A pitching-motion-activated flapping foil was also analyzed near a solid wall and between parallel walls using the Immersed Boundary-Lattice Boltzmann Method (Wu et al., 2014a). It was shown that, for a given amplitude and frequency, as the clearance decreases the net power extraction efficiency improves. They also observed that the leading edge vortex (LEV) from the foil between the parallel walls interacts with a wall vortex, enhancing lift.

Few previous experiments and simulations distinguish between 2-D and 3-D wall effects. Mivehchi et al. (2016) experimentally found that ground effect is markedly different in the two-dimensional case compared with the three-dimensional case based on force analysis. Perkins et al. (2018) also showed the difference of the 2-D and 3-D wall effect on the force characteristics using a rolling and pitching foil which is a more realistic 3-D configuration for underwater

vehicles. However, forces are integrated quantities, so it is necessary to observe the dynamic evolution of the wake in order to explain a dynamic ground effect in general. Understanding wake behavior in numerical simulations is valuable since the experimental setup in Mivehchi et al. (2016) does not allow for flow visualization of the 2-D tip configuration. In this study, wake information will be provided through the use of a real-time numerical simulation. A series of numerical experiments employing flapping foil kinematics replicate previous physical experiments (Mivehchi et al., 2016), and the numerical simulation supplement the previous experiments, providing visualization of the wake dynamics. Additionally, the 2-D simulations are compared with a Particle Image Velocimetry (PIV) from a 3-D experiment to characterize the fundamental differences in wall effect between 2-D and 3-D tip conditions.

Reference	Dim.	Foil Type	Re	Motion
Molina and Zhang (2011)	2D	Race Car Spoiler	3.9×10^4	Heave only
Liang et al. (2014)	2D	NACA0015	7.0×10^4	Heave only
Wu et al. (2014)	2D	NACA0015	1.1×10^3	Heave and pitch
Current work	2D	NACA0012	500	Heave and pitch

Table 1.1: Existing numerical study literatures

1.3 Methodology

1.3.1 Flapping foil motion near a flat wall

A two-dimensional NACA0012 foil with heave and pitch motion is used to investigate wall effect on the 2-D foil. The foil kinematics and geometry of the experiment are defined according to Licht et al. (2010) and Mivehchi et al. (2016)

as shown in figure 1.1. The pitch and angle of attack are sinusoidal functions:

$$\theta(t) = \theta_0 \, sin(\omega t) \tag{1.1}$$

$$\alpha(t) = \alpha_0 \, sin(\omega t) \tag{1.2}$$

Heave velocity is determined by the instantaneous pitch angle and angle of attack as expressed in the following equation:

$$\dot{h}(t) = U \tan(\alpha_0(t) - \theta_0(t)) \tag{1.3}$$

Heave position is determined through integration of equation (1.3):

$$h(t) = H + \int_0^t \dot{h}(t) dt \tag{1.4}$$

$$h_0 = h_{\max} - h_{\min} \tag{1.5}$$

Since the pitch and the angle of attack are sinusoidal functions in time, the heave position $h(t)$ is not a sinusoid. To obtain the desired heave amplitude, defined as the equation (1.5), the pitch amplitude θ_0 is determined computationally in iterations following the procedure in Licht et al. (2010) and Mivehchi et al. (2016).

Table 1.2 represents the non-dimensional parameters in the numerical simulation. Strouhal numbers in the range of 0.3 to 0.5 and the maximum angle of attack α_0 in the 15 to 45 degree range are tested in order to match the experimental conditions from Mivehchi et al. (2016). The mean heave distance to chord length H^* that is necessary to examine the wall effect on the flow around the foil varies from 1.33 to 6. A example of the foil kinematics is shown in figure 1.2.

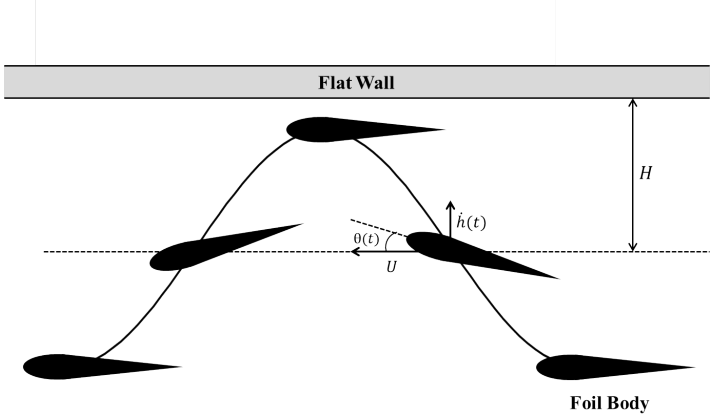

Figure 1.1: Schematic diagram of the flapping foil simulation

Reynolds number	$Re = \frac{Uc}{\nu}$	500
Strouhal number	$St = \frac{h_0 f}{U}$	$[0.3, 0.35, 0.4, 0.45, 0.5]$
Maximum nominal angle of attack	α_0	[15, 20, 25, 30, 35, 40, 45]
Heave amplitude to chord length	$h^* = \frac{h_0}{c}$	1
Mean heave distance to chord length	$H^* = \frac{H}{c}$	$[1.33, 1.66, 2, 3, 4, 5, 6]$
Pitch amplitude	θ_0	

Table 1.2: List of non-dimensional parameters and values in simulation

1.3.2 Numerical simulation

The Boundary Data Immersion Method (BDIM), developed by Weymouth and Yue (2011), is used to simulate the foil motion near a solid wall. This technique provides a robust and accurate solution of boundary conditions in solid/fluid interaction problems (Weymouth and Yue, 2011). The method is implemented in an open source program called LilyPad, which is run in Processing, a Java wrapper for visualization (Weymouth, 2015). Given fluid domain Ω_f and solid body domain Ω_b, the governing equations is incompressible Navier-Stokes equation for the fluid domain

$$\frac{\partial \vec{u}}{\partial t} + (\vec{u} \cdot \vec{\nabla})\vec{u} + \frac{1}{\rho}\vec{\nabla} p - \nu \nabla^2 \vec{u} = 0 \tag{1.6}$$

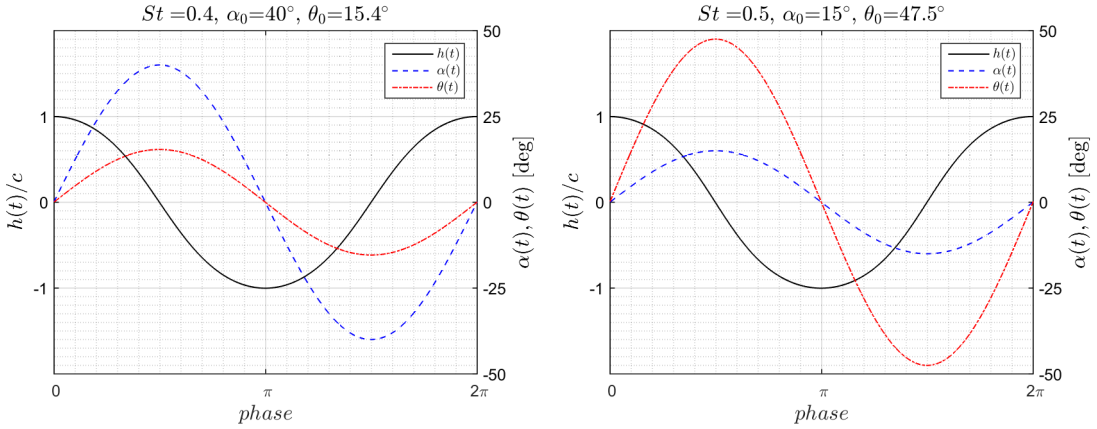

(a) (b)

Figure 1.2: Examples of the determined foil kinematics

and the boundary condition is simply

$$\vec{u} = \vec{V} \tag{1.7}$$

where $\vec{V}(\vec{x}, t)$ is prescribed velocity of the body. Both equations can also be written as different from by integration over a time step δt

$$\begin{cases} \vec{u} = \vec{b}, & \text{for } \vec{x} \in \Omega_b \\ \vec{u} = \vec{f}(\vec{u}), & \text{for } \vec{x} \in \Omega_f \end{cases} \tag{1.8}$$

where

$$\vec{b} = \vec{V} \tag{1.9a}$$

$$\vec{f}(\vec{u}, t_0 + \delta t) = \vec{u}(t_0) + \int_{t_0}^{t_0+\delta t} [-(\vec{u} \cdot \vec{\nabla})\vec{u} + \nu \nabla^2 \vec{u}] dt - \int_{t_0}^{t_0+\delta t} \frac{1}{\rho} \vec{\nabla} p dt \tag{1.9b}$$

Maertens and Weymouth (2015) described the evaluation of the convolution for the body equations 1.9a and 1.9b using the kernel in Figure 1.3, and obtained

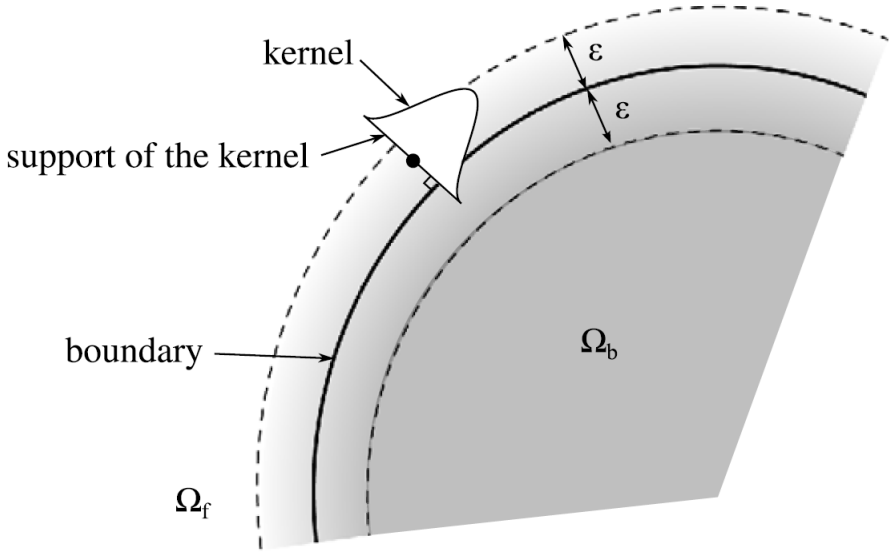

Figure 1.3: The immersed boundary with a kernel of radius ϵ for convolution of fluid and body equation (Maertens and Weymouth, 2015)

the meta-equation

$$\vec{u_\epsilon} = {\mu_0}^\epsilon \vec{f} + (1 - {\mu_0}^\epsilon)\vec{b} + {\mu_1}^\epsilon \frac{\partial}{\partial n}(\vec{f} - \vec{b}) \tag{1.10}$$

where ${\mu_0}^\epsilon$ and ${\mu_1}^\epsilon$ are the zeroth and first moments of the one-dimensional kernel over Ω_f, respectively. This meta equation is solved in LilyPad for flow velocity and pressure. Using a defined kernel and the signed distance $d(\vec{x})$ from $\vec{x}$ to the fluid-body boundary, the moments in the equation 1.10 are given by

$${\mu_0}^\epsilon = \begin{cases} \frac{1}{2}\Big[1 + \frac{d}{\epsilon} + \frac{1}{\pi}\sin\Big(\frac{d}{\epsilon}\pi\Big)\Big] & \text{for } |d| < \epsilon \\ 0 & \text{for } d \le -\epsilon \\ 1 & \text{for } d \ge \epsilon \end{cases} \tag{1.11a}$$

$${\mu_1}^\epsilon = \begin{cases} \epsilon\Big[\frac{1}{4} - \Big(\frac{d}{\epsilon}\Big)^2 - \frac{1}{2\pi}\Big(\frac{d}{\epsilon}\sin\Big(\frac{d}{\epsilon}\pi\Big) + \frac{1}{\pi}\Big(1 + \cos\Big(\frac{d}{\epsilon}\pi\Big)\Big)\Big)\Big] & \text{for } |d| < \epsilon \\ 0 & \text{for } |d| \ge -\epsilon \end{cases} \tag{1.11b}$$

From the 2-D numerical simulation, the instantaneous thrust (C_T) and lift coefficients (C_L) are obtained and analyzed. They are expressed as the equations 1.12 and 1.13:

$$C_T = \frac{F_x}{0.5\rho U^2 L} \tag{1.12}$$

$$C_L = \frac{F_y}{0.5\rho U^2 L} \tag{1.13}$$

where F_x and F_y are the instantaneous force in x and y direction, respectively. ρ is the fluid density, U is the uniform flow velocity, and L is the body resolution (chord length). To simplify, the time-averaged mean force coefficients are also calculated by the equations 1.14 and 1.15.

$$\bar{C}_T = \frac{\int_0^{n_c T} C_T dt}{n_c T} \tag{1.14}$$

$$\bar{C}_L = \frac{\int_0^{n_c T} C_L dt}{n_c T} \tag{1.15}$$

where n_c is the number of cycles and T is the period.

A convergence study was performed comparing the thrust and lift coefficients from flapping foil simulations with various resolutions. An experiment case is tested using the condition, $St = 0.4$, and $\alpha_0 = 40^\circ$ with the flapping foil operating in the freestream. The phase-averaged force coefficient profiles for each grid size ($1/n$) are obtained from the 5 cycles after the transient region of the simulation as shown in figure 1.4. To compare, Root Mean Squared Error (RMSE) with 72 phase average points of the profiles was calculated as:

$$RMSE = \sqrt{\frac{\sum_{i=1}^{n_s} (\hat{y}_i - y_i)^2}{n_s}} \tag{1.16}$$

where n_s is the number of sample points and $\hat{y}$ is the force coefficient value at the highest resolution($n = 2048$). Figure 1.5 shows the RMSEs for the thrust and lift coefficient profiles. The grid size 0.00098, which equals $n = 1024$, was chosen for subsequent numerical experiments with the $RMSE < 2\%$.

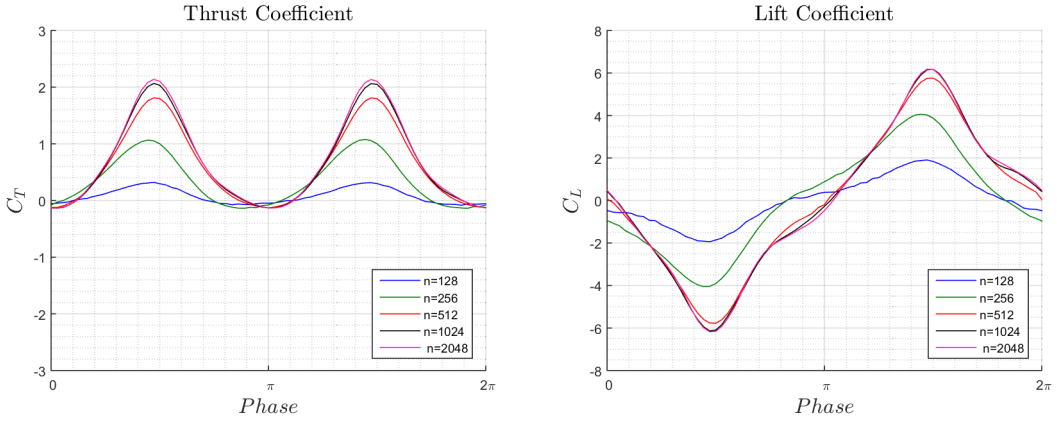

(a) Thrust Coefficient (C_T) (b) Lift Coefficient (C_L)

Figure 1.4: Force coefficients profiles for each grid size for convergence study ($St = 0.4, \alpha_0 = 40°$, No wall)

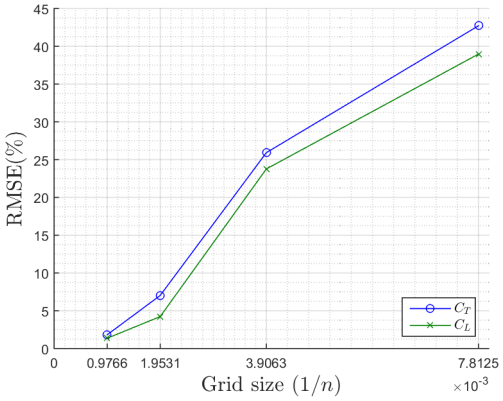

Grid Numbers $(n \times n)$	$RMSE_{C_T}$ (%)	$RMSE_{C_L}$ (%)
128×128	42.7	39.0
256×256	25.9	23.8
512×512	7.0	4.2
1024×1024	1.8	1.4

Figure 1.5: Root mean squared error for convergence study

Supplemental tests were performed to determine the fundamental parameters of simulation in LilyPad. The results from these tests were applied to all of the flapping foil simulation cases.

Transient Region The transient region at the beginning of the simulation was excluded from all of the results. To determine the region, the force profiles for each cycle were investigated in the same conditions in the convergence test. Figure 1.6 shows the varying force profiles along the cycles. The Root Mean Squared Error (RMSE) relative to the values of the next cycle was calculated with 72 points of the profiles. The cycles after the 5th cycle were taken as the results where the RMSEs, which were scaled by the maximum force coefficients, are less than 0.5% as shown in table 1.3.

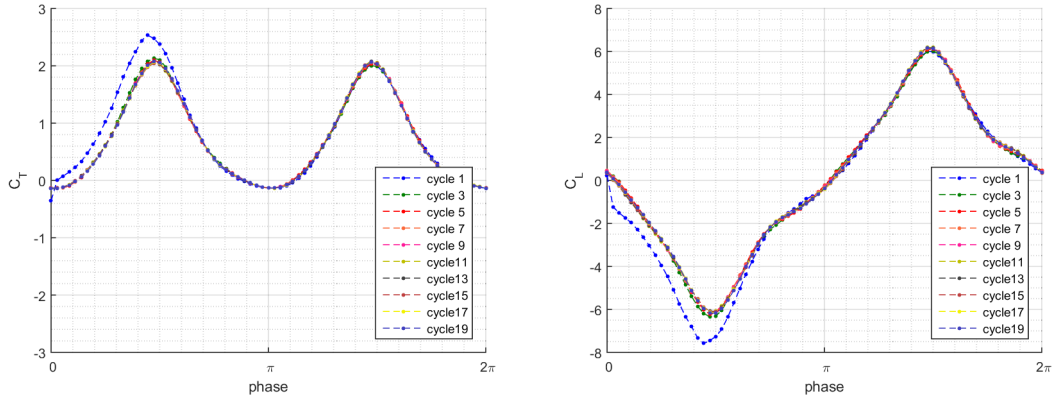

(a) Thrust Coefficient (C_T) (b) Lift Coefficient (C_L)

Figure 1.6: Force coefficients profiles and for each cycle ($St = 0.4, \alpha_0 = 40°$, No wall)

Cycle(i)	1	2	3	4	5	6	7	8	9
$RMSE_{C_T}$ (%)	7.34	1.41	0.74	0.42	0.28	0.19	0.20	0.19	0.19
$RMSE_{C_L}$(%)	9.68	2.19	1.16	0.61	0.44	0.37	0.37	0.34	0.37

Table 1.3: RMSE of thrust and lift coefficients for each cycle

Domain Size Since the top and bottom boundary conditions are considered as a wall in the simulation, the distance between the boundary and the foil body must be sufficient to avoid an unexpected ground effect. A test was performed to determine the domain size with the same conditions in the convergence study.

While the body resolution L is fixed, the grid numbers are changed according to domain size as described in Table 1.4. The mean heave distance from the top and bottom boundary is presented in the same table as well.

Body resolution (L)	Grid numbers($n \times n$)	Distance to Boundary
40	128×128	$1.6L$
40	256×256	$3.2L$
40	512×512	$6.4L$
40	1024×1024	$12.8L$
40	2048×2048	$25.6L$

Table 1.4: Test parameters to determine domain size

Figure 1.7 shows the change of the thrust and lift coefficient profiles for each simulation domain size. The Root Mean Squared Error (RMSE) for the 72 sample points of the profile was calculated using the equation 1.16. The RMSE is less than 2% when the domain size is 512×512 with the body resolution $L = 40$ as shown in Table 1.5. It shows that the flapping foil motion can be considered far enough away from the boundary with the domain size where the distance from the mean heave position of the foil body is greater than $6.4L$.

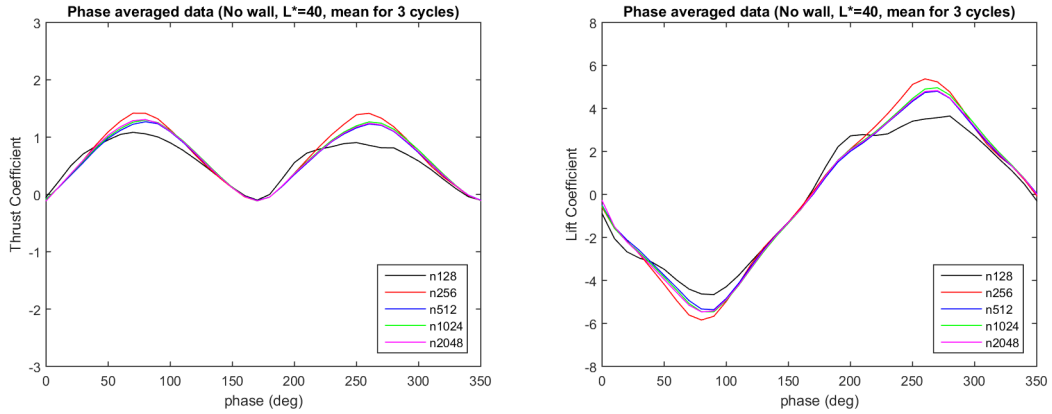

(a) Thrust Coefficient (C_T) (b) Lift Coefficient (C_L)

Figure 1.7: Force coefficients profiles for each domain size ($St = 0.4, \alpha_0 = 40°$, No wall)

Domain size ($n \times n$)	128×128	256×256	512×512	1024×1024
$RMSE_{C_T}$ (%)	12.78	5.71	1.82	1.40
$RMSE_{C_L}$(%)	11.91	5.52	1.97	1.63

Table 1.5: RMSE of thrust and lift coefficients for each domain size

Reynolds Number The simulation is conducted with a Reynolds number (Re) 500 included in the laminar flow, since the 2-D flow solver will more properly model turbulent effect at low Reynolds numbers. This is because of the turbulence characteristics at high Reynolds number, and it is not captured properly due to implicit 2-D representation of turbulence. The physical experiment is conducted in a turbulent condition, that is $Re = 21,000$. To study the effect of the Reynolds number on the simulation results, the vortices and the force profiles are compared between the simulations of $Re = 500$ and $Re = 21,000$ using the same kinematic parameters with the convergence study and adding a wall ($H^* = 4$).

Figure 1.8 shows the comparison of the wake at one time instant. The vortices shed near the foil body in the more turbulent wake ($Re = 21,000$) break into additional tiny vortices around the major vortices that are observed at the lower Reynolds number ($Re = 500$). Despite the difference in the number of vortices, the location and shape of the major vortices is consistent in the two simulation cases for Reynolds numbers 500 and 21,000. The thrust and lift coefficient profiles do not have significant discrepancies with minor fluctuations appearing in lift at higher Reynolds number and the low Reynolds number captures the mean behavior. Since Reynolds number is not found to significantly impact the observed forces compared with the higher Reynolds number case, a Reynolds number of 500 was used to limit computational time.

Viscous Force The force exerted on the flapping foil in the numerical simulation is calculated based on the pressure and shear stress around the body. The effect of

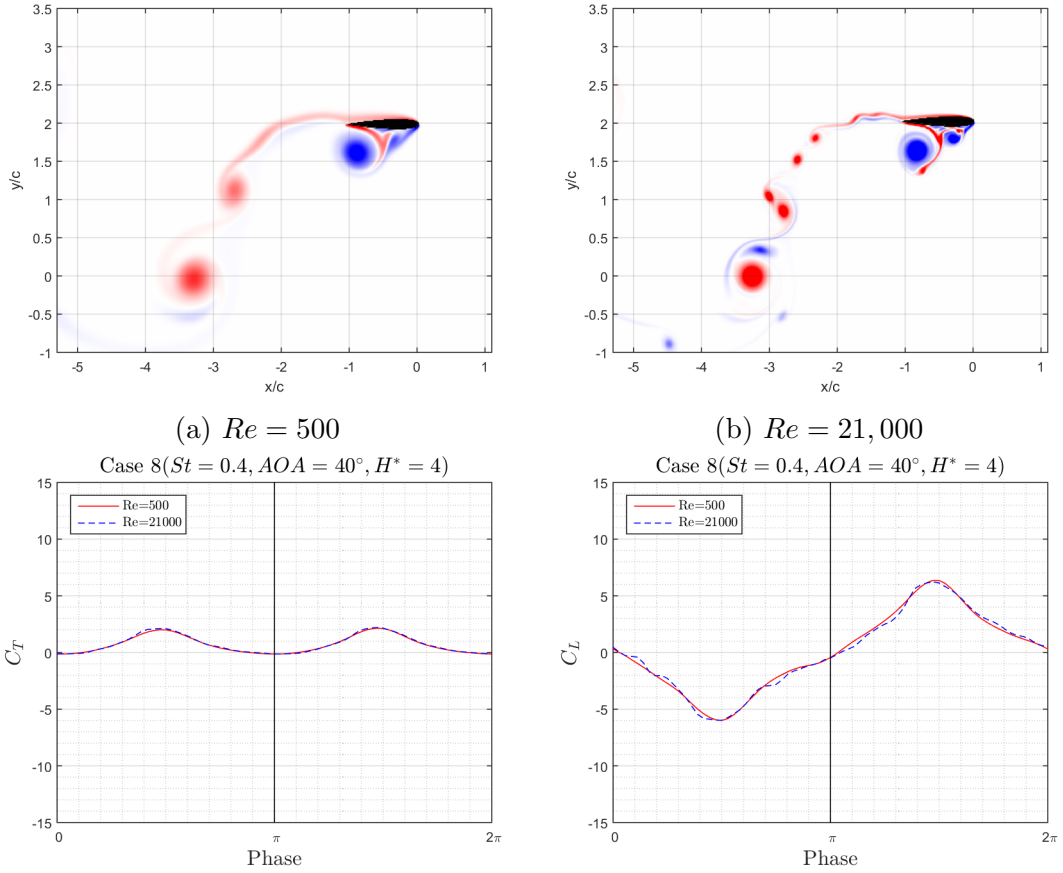

(a) $Re = 500$ (b) $Re = 21,000$

(c) C_T Comparison (d) C_L Comparison

Figure 1.8: Comparison of vorticity plots and force profiles between Reynolds number 500 and 21,000 ($St = 0.4, \alpha_0 = 40°, H^* = 4$)

the viscous forces on the force profiles is investigated through a static foil simulation with 0° of angle of attack and a case of the flapping foil simulation, $St = 0.4, \alpha_0 = 40°$. The skin friction force $\vec{F_f}$ on the body is computed as:

$$\overrightarrow{F_f} = \int_{\Omega} \rho \, \nu \, \hat{n} \cdot (\overrightarrow{\nabla} \overrightarrow{u} + \overrightarrow{\nabla} \overrightarrow{u}^T) \, d\overrightarrow{x} \tag{1.17}$$

Figure 1.9 shows the pressure and friction drag force coefficients of the hydrofoil simulation for a body resolution, $L = 102.4$ and 204.8. Table 1.6 shows total drag coefficients C_D of the simulation at each body resolution, $L = 51.2, 102.4, 204.8$, and also shows the pressure drag coefficient C_{Dp} and the

friction drag coefficient C_{Df}, respectively. The total drag coefficients in other references are listed for comparison. The simulation results show that the friction drag coefficient has a relative error of 10.9% with the body resolution, $L = 102.4$, and may require a higher resolution simulation for the correct evaluation of the friction force. The discrepancy of the total drag coefficient C_D with the other studies is observed.

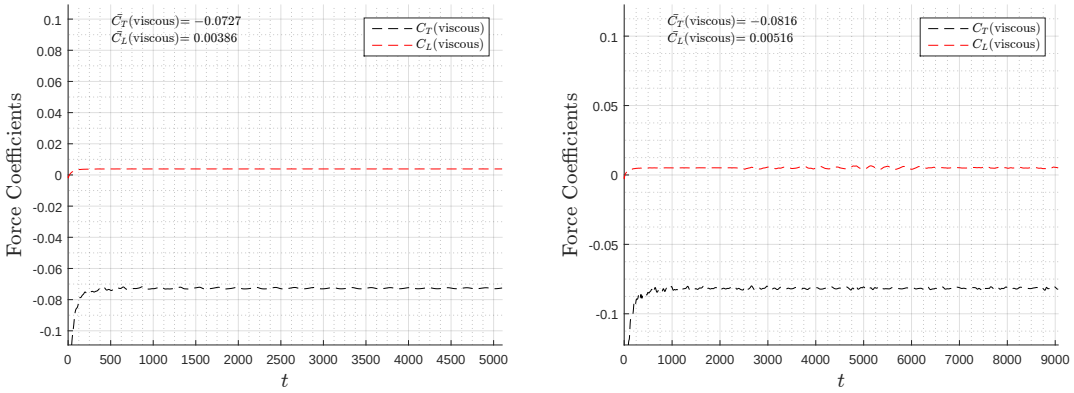

(a) $L = 102.4$ (b) $L = 204.8$

Figure 1.9: Friction force coefficients of the static NACA0012 simulation at 0° of angle of attack (Re=500)

	Re	C_D	C_{Dp}	C_{Df}	Remarks
	500	0.0988	0.0401	0.0587	$L = 51.2$
		(20.3%)	(5.64%)	(28.1%)	
Present	500	0.114	0.0418	0.0727	$L = 102.4$
		(8.06%)	(1.65%)	(10.9%)	
	500	0.124	0.0425	0.0816	$L = 204.8$
Lockard et al. (2002)	500	0.1762	-	-	Numerical (CFL3D)
Imamura et al. (2005)	500	0.1725 -	-	-	Numerical (GILBM)
Pantula (2008)	500	0.1739	-	-	Numerical (FD-IB)

*Relative errors in parentheses

Table 1.6: Comparison of drag coefficients of NACA 0012 with 0° of angle of attack

The flapping foil simulations are performed without a wall including the viscous force. Figure 1.10 shows the force coefficients of the simulation without a wall at the body resolution $L = 80$ and 160. The change in the pressure force profiles by the viscous force is marginal since the pressure force is dominant in the flapping foil motion; otherwise, the friction force is dominant in the static foil simulation. To limit the computational time, the viscous force on the flapping foil simulation is excluded as it requires much high body resolution for an accurate solution.

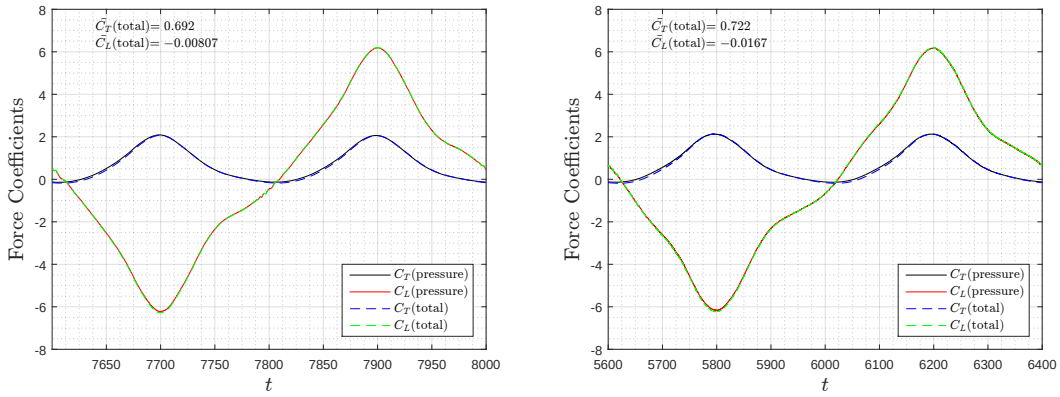

(a) $L = 80$ (b) $L = 160$

Figure 1.10: Force coefficients of the flapping NACA0012 simulation without wall. The kinematic parameters for the case 8 are used; Strouhal number $St = 0.4$, and the maximum angle of attack $\alpha_0 = 40°$.

In this research, all numerical experiments are conducted with the settings as shown in table 1.7. The n is the number of grid cells for each direction and the body resolution L is a non-dimensional parameter that is defined as the number of grid points along the body.

1.3.3 Validation

The validation of simulation results was conducted by comparing them with effective 2-D experimental data. Read et al. (2003) performed an approximated 2-D experiment with flapping NACA 0012 foil using endplates at the ends of the

Reynolds Number (Re)	500
Grid Numbers ($n \times n$)	$2^{10} \times 2^{10}$
Body resolution (L)	80

Table 1.7: Fundamental parameters for the numerical experiments

foil to prevent the span-wise flow. The contour plots of the mean thrust and coefficients are shown as a function of Strouhal number and the maximum angle of attack in Figure 1.11. The shaded region in Figure 1.11(b) is the range of numerical simulations and they are well matched. Additionally, the mean lift coefficients in the simulation are close to zero in all of the cases when the mean heave distance, H^*, is equal to 6. This is an expected result as no wall effect should exist where the foil is distant from the wall.

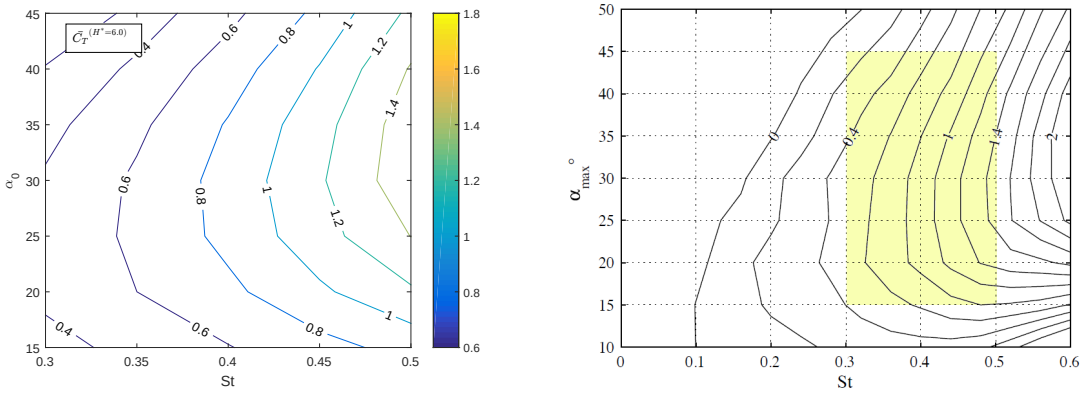

(a) Current ($H^* = 6$) (b) Read et al. (2003)

Figure 1.11: Comparison of time averaged thrust coefficients $\bar{C}_T$ with respect to Strouhal number and maximum angle of attack

1.3.4 Particle Image Velocimetry (PIV)

To compare the 2-D numerical simulation with the 3-D experiment, particle image velocimetry (PIV) data was used. The technique conventionally employs two cameras to record the specific region of interest to identify changes in flow structures. By calculating the correlation of the position of the particles captured

by two images, we can identify the direction and magnitude of the velocity vector. The PIV experiments were conducted in the cases of Mivehchi et al. (2016) where Reynolds number $Re = 20,000$, Strouhal number $St = 0.4$ and maximum angle of attack $\alpha_0 = 40°$. The mean heave distance from the wall $H^* = 1.33$ and 4 were used to investigate the ground effect.

1.4 Results

The instantaneous force coefficient profiles during a full cycle from the 2-D numerical simulation are represented and compared with those from the 3-D experiment. The profile data is phase-averaged over the five cycles of the flapping motion while the transient region in the simulation and the experiment is examined and excluded from the data. The solid line in Figure 1.12 and 1.13 is the 2-D simulation result of the thrust and lift coefficient profiles in the different cases in the range of $St = 0.3$ to 0.5, $\alpha_0 = 20°$ to $40°$ at $H^* = 4$. The dashed line represents the corresponding results from the 3-D experiment in Mivehchi et al. (2016). The thrust and lift coefficients, C_T and C_L, respectively, show that the expected profiles are similar to the experiment and other previous flapping foil motion research. The foil travels toward the wall during the first half-cycle and travels away from the wall during the second half-cycle. The peaks of the thrust and lift coefficients are observed at the phase of $\frac{1}{4}\pi$ and $\frac{3}{4}\pi$ where the angle of attack $\alpha(t)$ is maximum.

The difference between the profiles in the 2-D simulation and the 3-D experiment are also observed such that the peak thrust amplitude in the second half-phase is markedly larger in the experiment than in the simulation. The lift coefficient profiles also have differences in the peak magnitude and the profile behavior with a fluctuation in the 3-D experiment results. The discrepancies are generally larger in the high Strouhal number (St) cases. Otherwise, phase shift

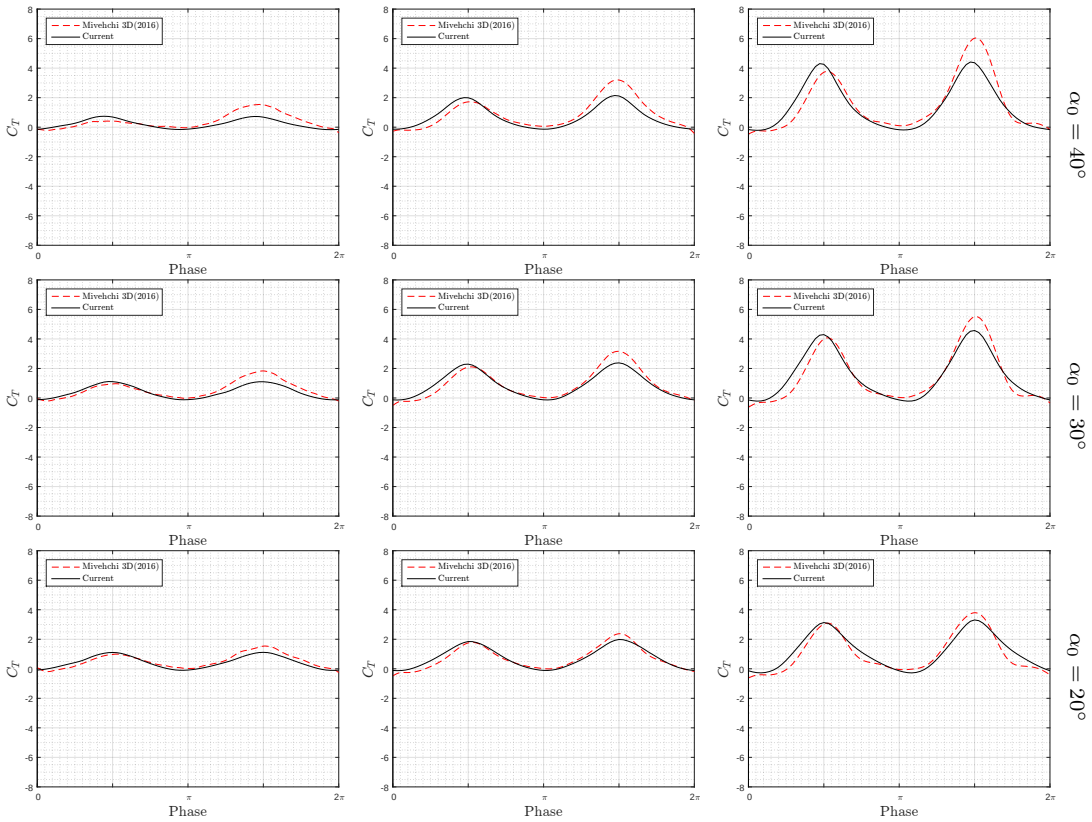

Figure 1.12: Comparison of thrust coefficient (C_T) profiles between the 2-D simulation and the 3-D experiment ($H^* = 4$)

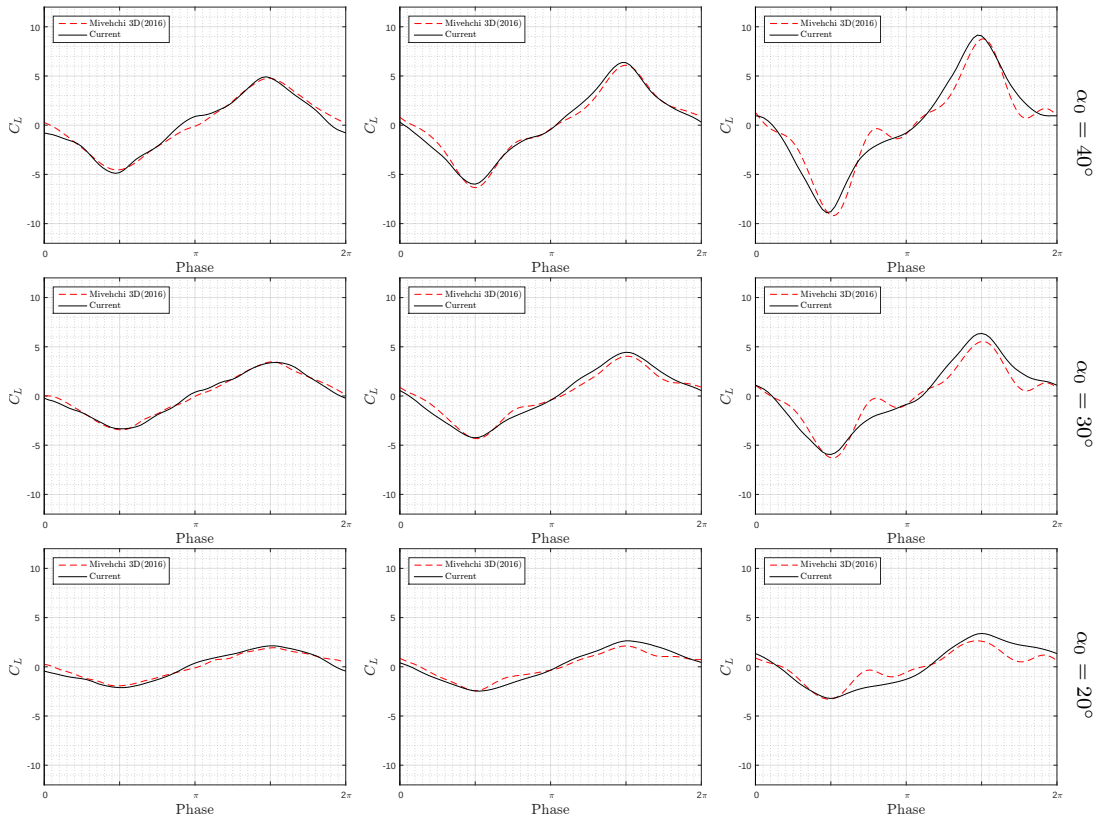

Figure 1.13: Comparison of lift coefficient (C_L) profiles between the 2-D simulation and the 3-D experiment ($H^* = 4$)

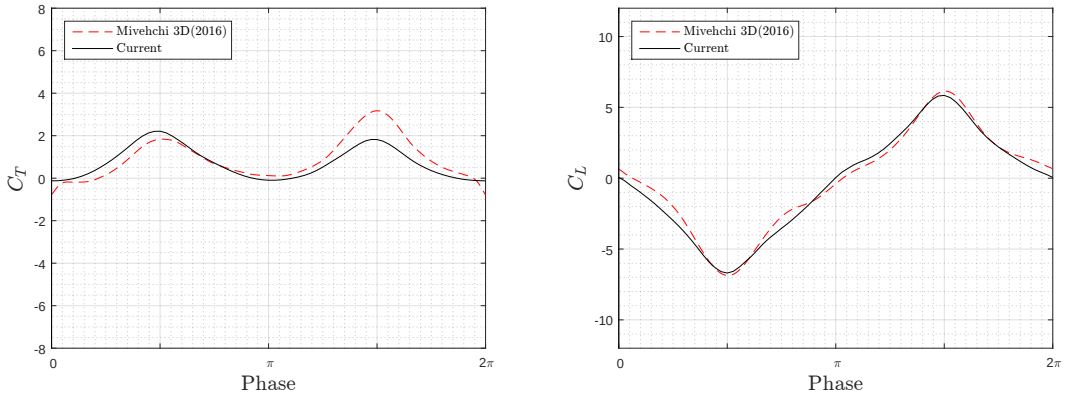

(a) Thrust coefficient ($H^* = 1.33$)

(b) Lift coefficient ($H^* = 1.33$)

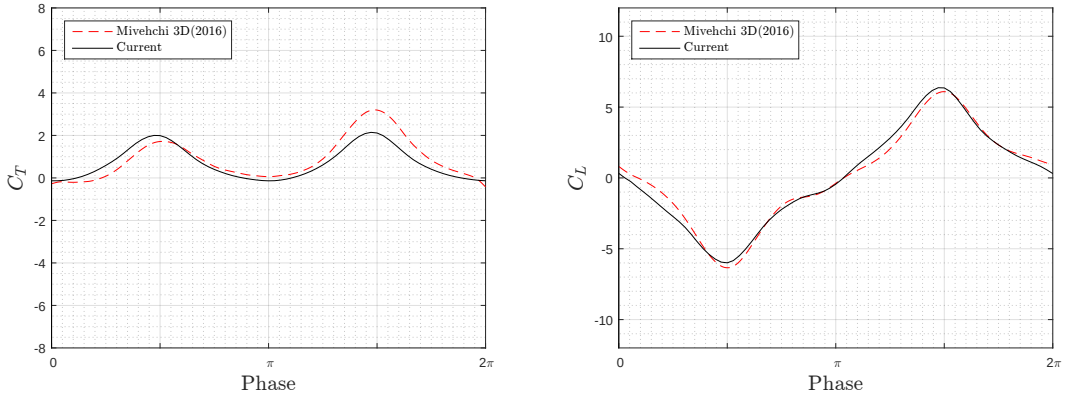

(c) Thrust coefficient ($H^* = 4$)

(d) Lift coefficient ($H^* = 4$)

Figure 1.14: Comparison of force coefficient profiles between the 2-D simulation and the experiments with the different mean heave distance $H^* = 1.33$ and 4 in the case of $St = 0.4$, $\alpha_0 = 40°$

in the first half-phase is found especially with the high maximum angle of attack (α_0). Figure 1.14 shows the effect of the wall on the force profiles in the simulation and experiment in the case of $St = 0.4$ and $\alpha_0 = 40°$, with the different mean heave distance $H^* = 1.33$ and 4. In the 2-D simulation results, asymmetric peak force magnitude is observed in the wall case ($H^* = 1.33$), compared with the away case ($H^* = 4$). The thrust and lift peaks are altered in the first half cycle, when the foil moves toward the wall. The 3-D experiment shows the same change in the lift coefficient profile, but it is marginal in the thrust coefficient.

Change in the behavior of the vortices in time behind the flapping foil were

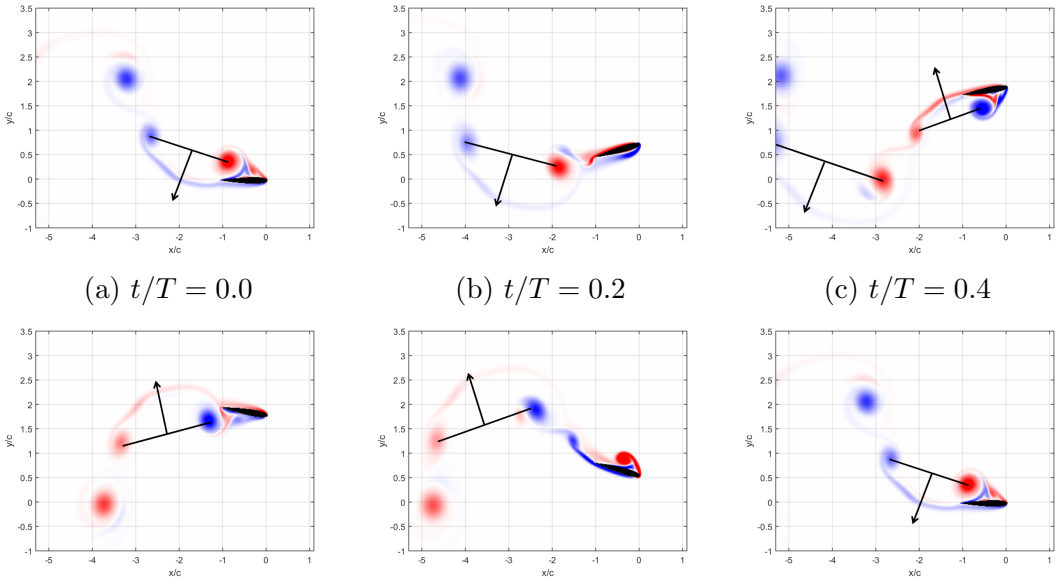

(a) $t/T = 0.0$ (b) $t/T = 0.2$ (c) $t/T = 0.4$

(d) $t/T = 0.6$ (e) $t/T = 0.8$ (f) $t/T = 1.0$

Figure 1.15: Time series images of vortex shedding behind flapping foil motion in 2-D numerical simulation ($H^* = 4$)

observed in the range of $x/c = -5$ to 1 and $y/c = -1$ to 3.5 where the location of the nose of the foil is at $x/c = 0$ and $y/c = 0$. Figure 1.15 shows the time series images of the vortex shedding in the 2-D simulation in the case of $H^* = 4$. It represents the four vortices from each cycle, one leading edge and one trailing edge vortex for each half cycle. Arrows are drawn from the mid-point of each vortex pair to indicate the direction of flow. The reverse *von Kármán* vortex, which induces thrust force, is clearly observed as in Anderson et al. (1998). The vortex pair of the leading edge and the trailing edge vortex are symmetrical according to the foil motion. The pattern of the vortex has been shown in previous numerical studies (Liang et al., 2014; Molina and Zhang, 2011).

Figure 1.16 shows that the presence of the wall alters the wake formation of the flapping foil. A leading edge vortex (blue color) is developed in figure 1.16(c) and forms a vortex pair with a trailing edge vortex (red color). In figure 1.16(e), the leading edge vortex interacts with the wall and is combined with the following

trailing edge vortex. The combination of vortices is clearly observed in figure 1.16(f) and also changes the flow direction between the vortex pairs. This is a distinguishable characteristic in the wall case of the 2-D numerical simulation.

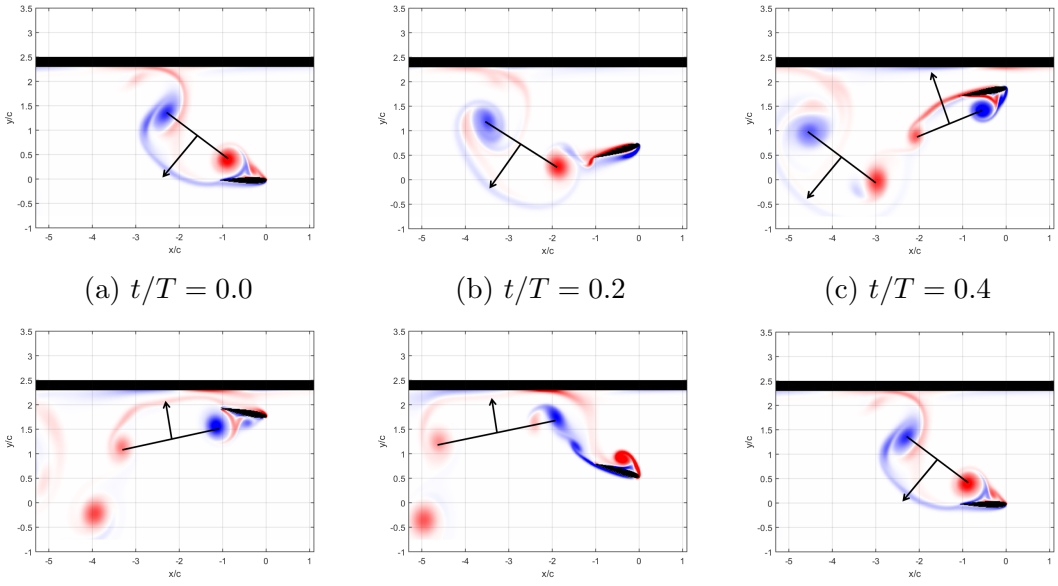

(a) $t/T = 0.0$ (b) $t/T = 0.2$ (c) $t/T = 0.4$

(d) $t/T = 0.6$ (e) $t/T = 0.8$ (f) $t/T = 1.0$

Figure 1.16: Time series images of vortex shedding behind flapping foil motion in 2-D numerical simulation ($H^* = 1.33$)

From the 3-D experiment, three locations of slice PIV data at $z/c = 0.5$, 0.25, and 0 were taken where z/c is the span-wise position on the foil body from the tip. Figures 1.17 and 1.18 represent a comparison between the 2-D and 3-D images at the normalized time $t/T = 0.0$ to 0.8 in a completed cycle. When the 2-D and 3-D cases are compared, the vortex behavior in 2-D numerical simulation is significantly different from those of 3-D cases at $z/c = 0$ and 0.25 in terms of location and shape of the vortices. The vortices shedding in the 3-D case at $z/c = 0.5$ are similar with that of the 2-D case, but still have discrepancies. A cross section of the vortex with respect to the x-axis is observed at the tip ($z/c = 0$) of the 3-D PIV slice data. The shape of the leading edge vortex (LEV) is observed clearly as that of a circle in 2-D simulation while appearing dispersed in the 3-D example at $z/c = 0.5$. The

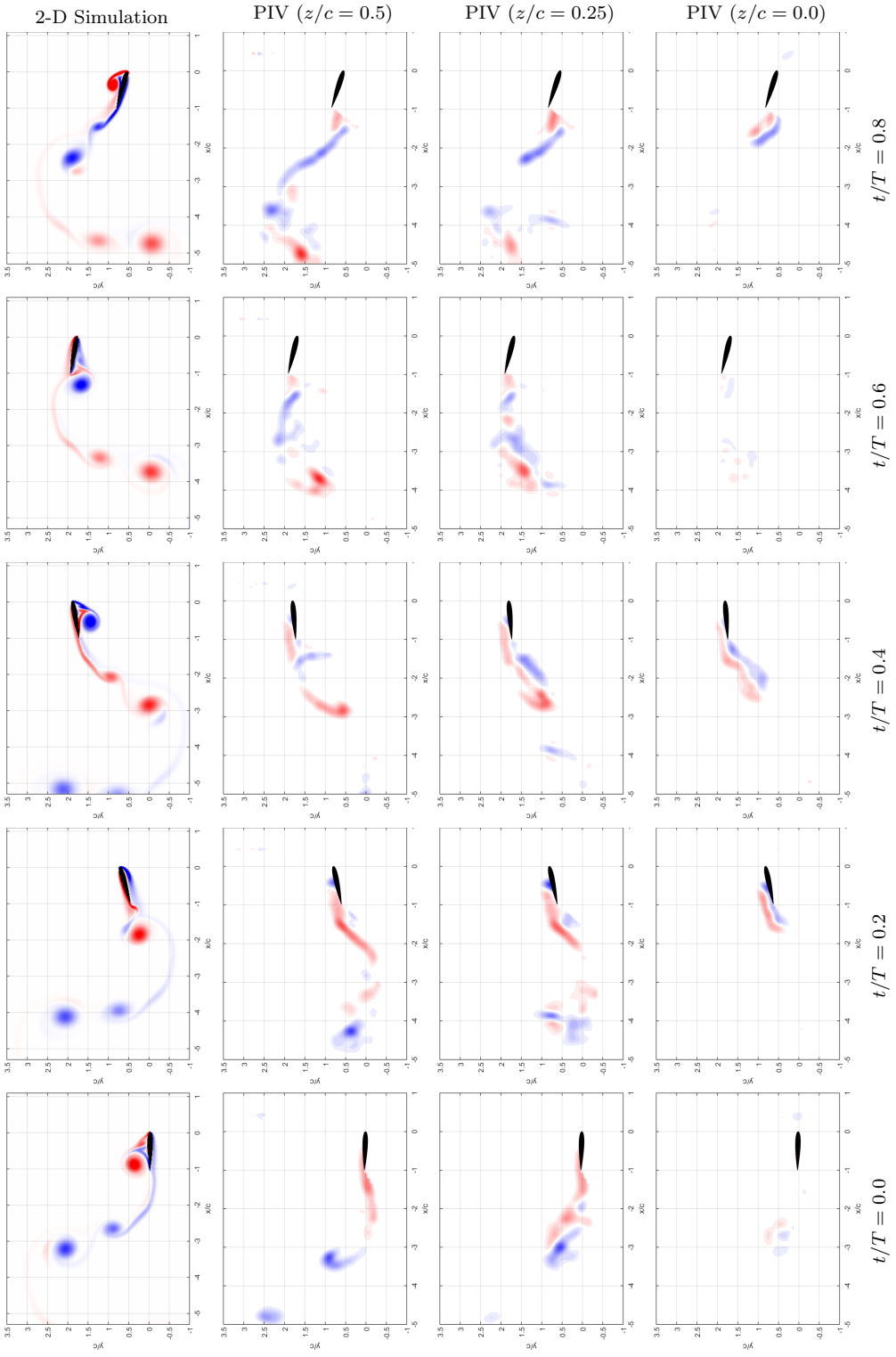

Figure 1.17: Time series images of vortex shedding behind flapping foil motion in 2-D numerical simulation and 3-D experiment PIV data in the away case ($H^* = 4, St = 0.4, \alpha_0 = 40°$). The PIV data is represented at the three different position $z/c = 0.5, 0.25, 0.0$ from the tip of the foil body.

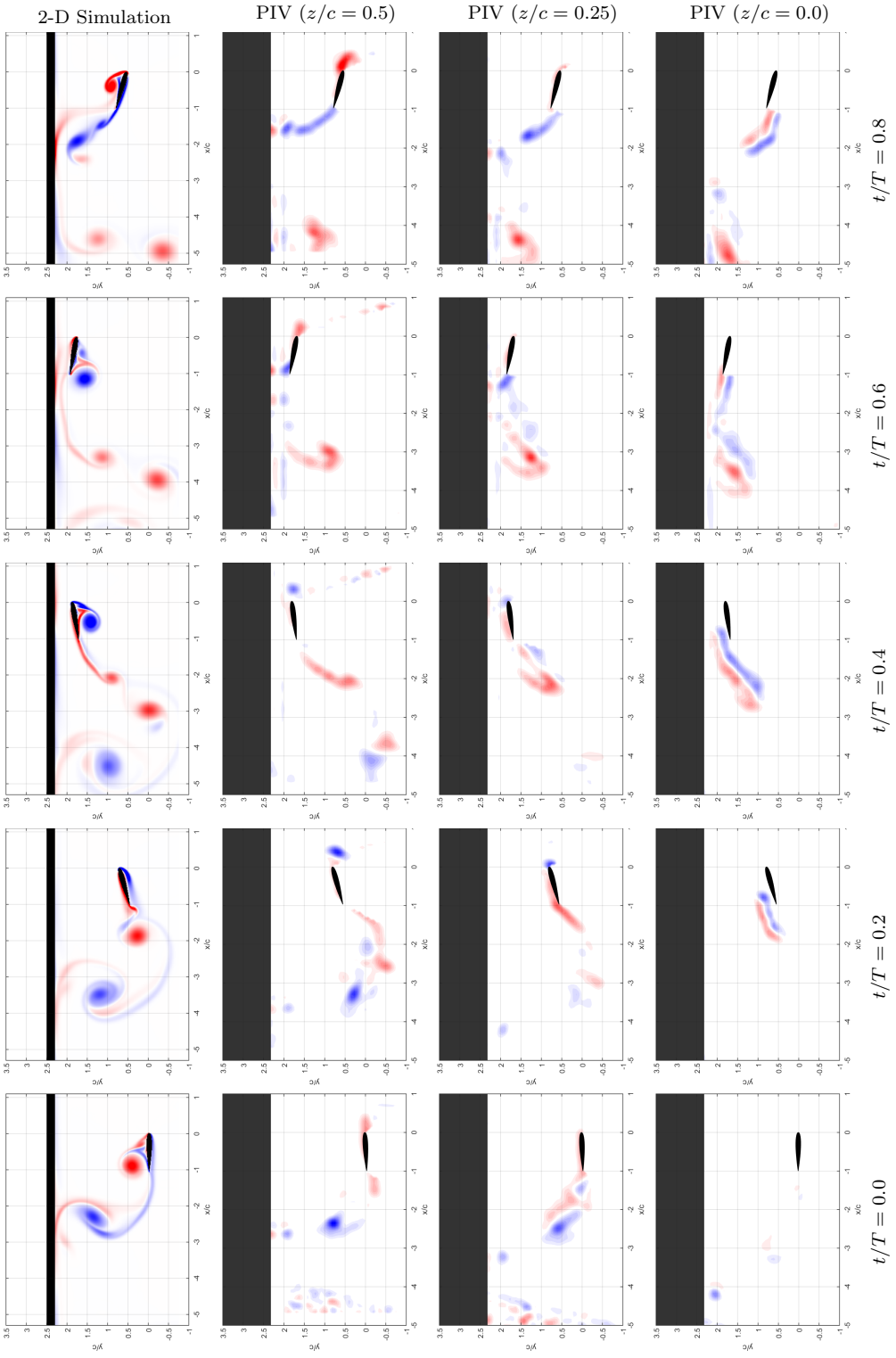

Figure 1.18: Time series images of vortex shedding behind flapping foil motion in 2-D numerical simulation and 3-D experiment PIV data in the wall case ($H^* = 1.33, St = 0.4, \alpha_0 = 40°$). The PIV data is represented at the three different position $z/c = 0.5, 0.25, 0.0$ from the tip of the foil body.

distance between the vortex pair in the 3-D case at $z/c = 0.5$ is smaller than in the 2-D case.

1.5 Discussion

1.5.1 Vortex at the tip of the foil in 3-D Case

The difference of vorticity plot between the 2-D simulation and 3-D experiment explains the discrepancies in force coefficient. A time-variant vortex occurs at the tip of the foil ($z/c = 0$) in the 3-D experiment when the angle of attack of the foil body is non-zero as shown in figure 1.19. This vortex produces a span-wise velocity which causes the significantly different vortex behavior as opposed to that of the 2-D numerical simulation.

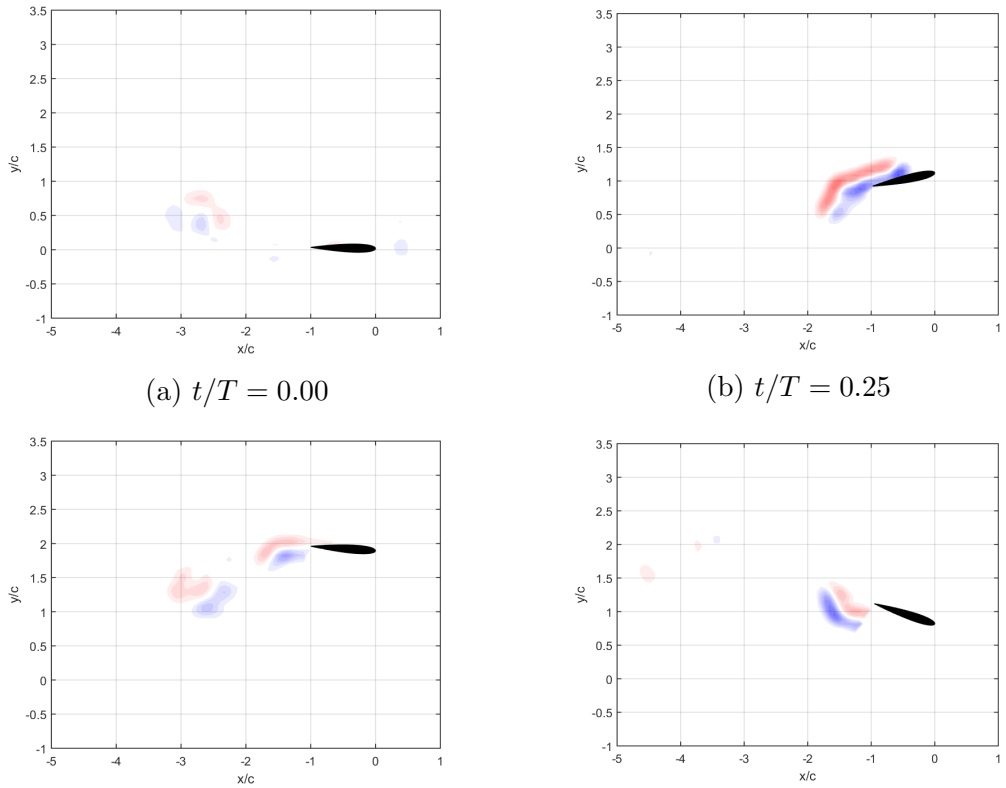

(a) $t/T = 0.00$ (b) $t/T = 0.25$

(c) $t/T = 0.50$ (d) $t/T = 0.75$

Figure 1.19: Development of the vortex at the tip ($z/c = 0$) in the 3-D PIV experiment in the case of $St = 0.4$, $\alpha_0 = 40°$, $H^* = 4$

Figure 1.19 shows the strength of the vortex at the tip is strongest when the angle of attack of the foil is at its maximum (at $t/T = 0.25, 0.75$), and weakest when the angle of attack is zero (at $t/T = 0.0, 0.5$). This also explains why the discrepancy in the force magnitude is largest at $t/T = 0.25, 0.75$, as presented in Figure 1.14. Leading edge vortex (LEV) in the flapping foil motion is clearly observed when the angle of attack is larger than 10° (Anderson et al., 1998). In this study, the LEV (red color) at $z/c = 0.5$ is possibly dispersed by the spanwise velocity from the tip. The dispersion of LEV leads the vortex to shift to backward, as shown in Figure 1.20. The PIV image data is only obtained at the three locations of $z/c = 0, 0.25$, and 0.5 from the tip of the foil, thus it was not investigated where the vortical pattern is not altered by the tip flow.

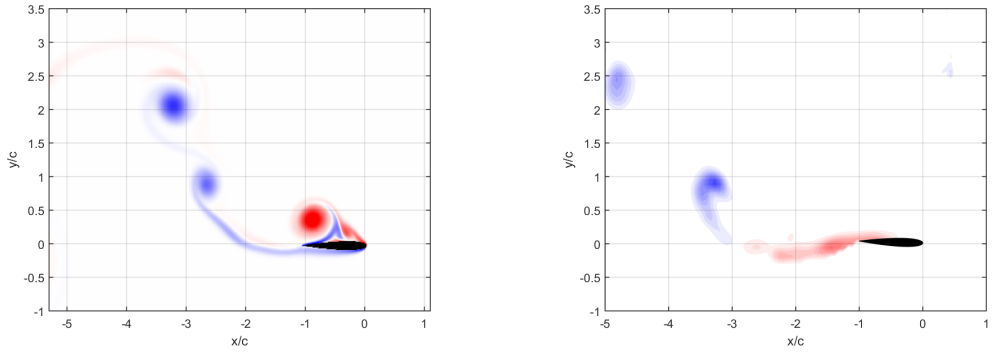

(a) 2D Simulation (b) 3D PIV ($z/c = 0.5$)

Figure 1.20: A shifting of the vortex of the pair behind the foil by the dispersion of leading edge vortex (LEV) in the away case ($H^* = 4$) at a time instant $t/T = 0.0$

1.5.2 Wall effect in 2-D and 3-D case

The existence of the wall near a flapping foil motion causes change in the location of vortices shedding behind the foil. As shown in figure 1.21, the trailing edge vortex of the pair is shifted to the right side by the wall in both the 2-D and 3-D cases at $z/c = 0.5$. This provides a change in the distance and direction between the vortex pair that produces different hydrodynamic force characteristics. In the

3-D PIV experiment, no combination of two blue vortices is presented, as opposed to the 2-D simulation case. This could be one reason why the force coefficients in Figure 1.14 have a different phase behavior around $t/T = 0.0$ between the simulation and the experiments.

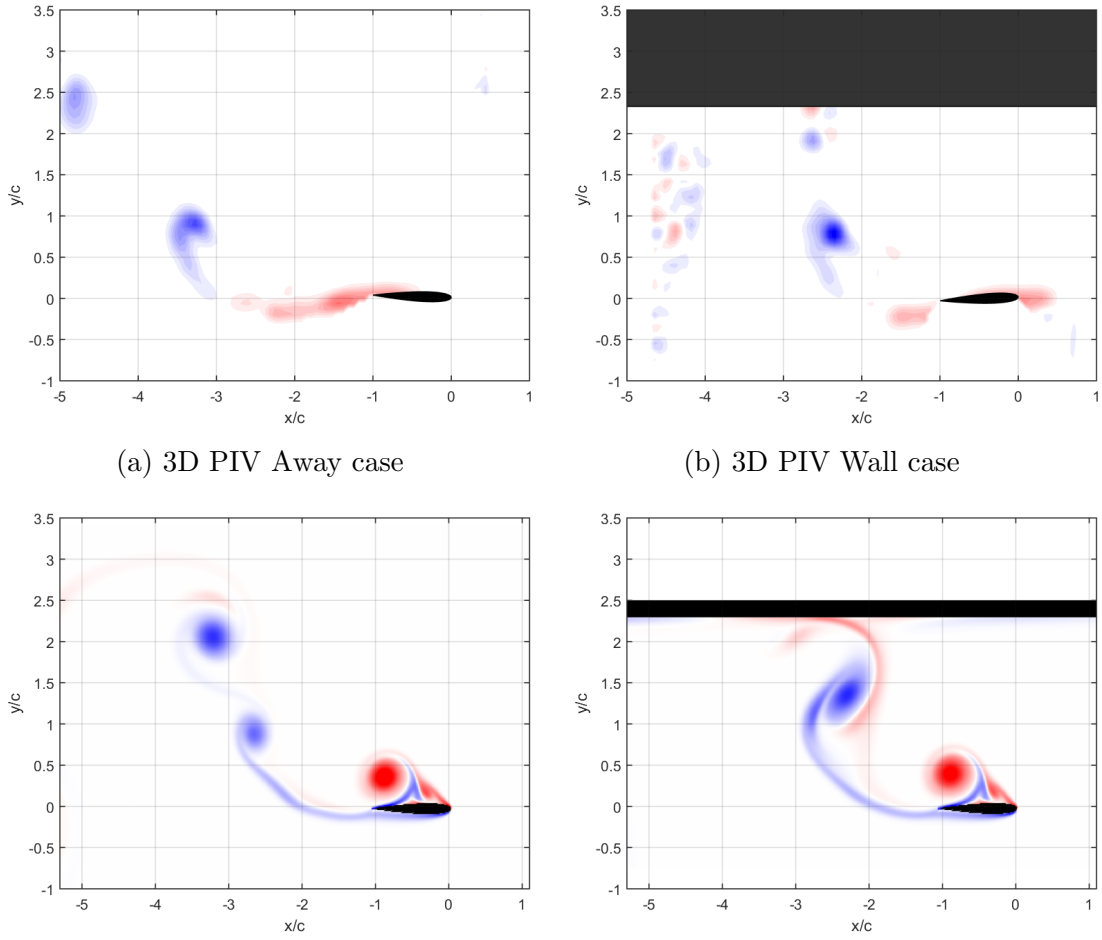

(a) 3D PIV Away case

(b) 3D PIV Wall case

(c) 2D Simulation Away case

(d) 2D Simulation Wall case

Figure 1.21: Wall effect on the vorticity plot in 2-D simulation and 3-D PIV experiment at $z/c = 0.5$ ($St = 0.4$, $\alpha_0 = 40°$, $t/T = 0.0$)

Furthermore, the wall effect is observed in the vorticity plot at the tip location ($z/c = 0$) of 3D PIV data. Figure 1.22 shows the vortex development at the tip during the normalized time $t/T = 0.4$ to 0.6 in the away and the wall case. At $t/T = 0.5$, the angle of attack of the foil is zero and the vortex at the tip is

weakened and disappears as shown in Figure 1.22(a), (b), and (c). On the other hand, the vortex maintains the strength when the wall exists. Figure 1.22(d), (e), and (f) presents that the vortex at the tip does not disappear near the wall. The presence of the vortex at the tip makes the difference between the 2-D simulation and 3-D experiment. Hence, this wall effect on the vortex at the tip explains why the discrepancy in the lift coefficients of the first half cycle is larger in the wall case ($H^* = 1.33$) than in the away case ($H^* = 4$) as shown in Figure 1.14. These characteristics of the wall effect on the vortex also depend on the foil kinematics such as Strouhal number and the maximum angle of attack. In this study, the PIV visualization data is limited to a particular case of the foil kinematics; hence, the comparison of the vortex behavior in the wall effect is not covered widely.

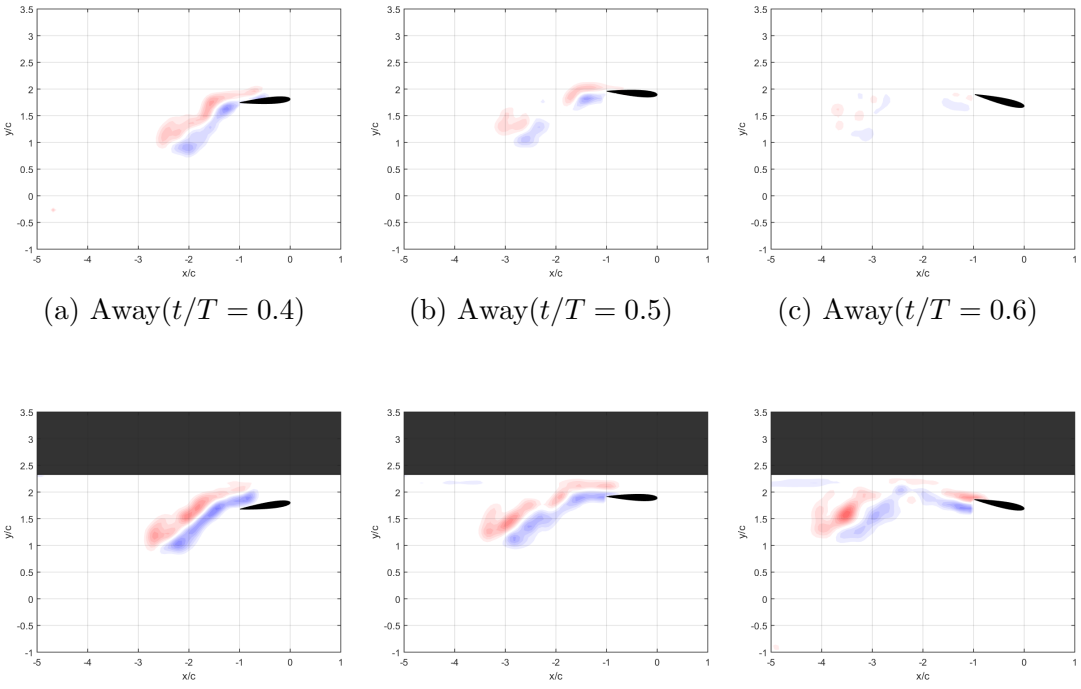

(a) Away($t/T = 0.4$) (b) Away($t/T = 0.5$) (c) Away($t/T = 0.6$)

(d) Wall($t/T = 0.4$) (e) Wall($t/T = 0.5$) (f) Wall($t/T = 0.6$)

Figure 1.22: Vortex development of 3D PIV experiment at the tip of the foil in the away and wall case ($St = 0.4$, $\alpha_0 = 40°$)

1.5.3 Peak location in thrust coefficient profile

The magnitude of force coefficients is asymmetric at the 1st and the 2nd half phase when the wall exists ($H^* = 1.33$) as shown in Figure 1.14. The experiment (Mivehchi, 2016) has consistent maximum peak position in the thrust coefficient. Otherwise, the thrust coefficients in the 2-D numerical simulation have different peak positions according to Strouhal number and maximum angle of attack. Figure 1.23 represents the examples of the thrust coefficient profile in the two different cases.

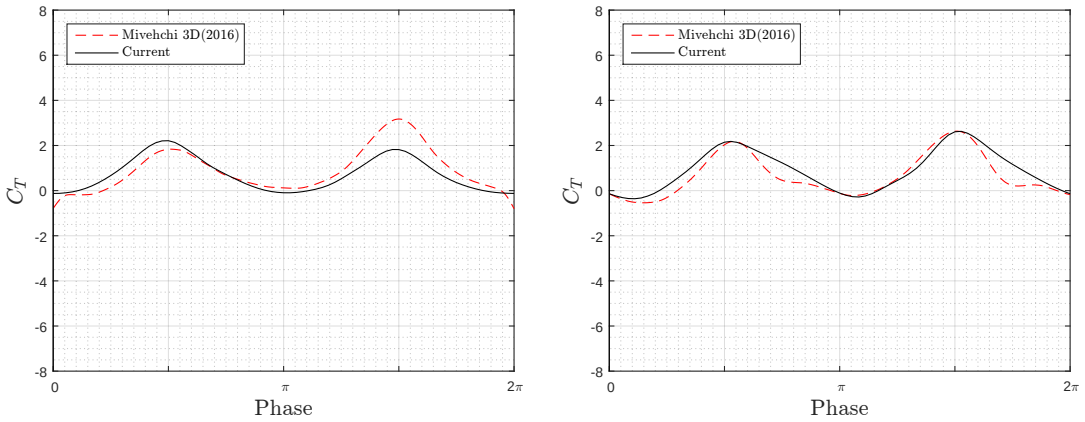

(a) $St = 0.4, \alpha_0 = 40°$ (b) $St = 0.5, \alpha_0 = 15°$

Figure 1.23: A discrepancy of maximum peak location in thrust coefficient (C_T) profiles ($H^* = 1.33$)

In the numerical simulation, as shown in figure 1.23 and table 1.8 , the maximum peak is located in the 1st half cycle with low Strouhal number and high angle of attack while the peak is in the 2nd half cycle with high Strouhal number and low angle of attack. In the experiment, the maximum peak is consistently in the second half cycle. The maximum thrust peak position in the first half cycle, when the foil moves toward the wall, is possibly an inherent characteristic of the 2-D numerical simulation.

Figure 1.24 shows the vortex formation of the 2-D numerical simulation and the 3-D PIV experiment in the case of high angle of attack and low Strouhal

$H^* = 1.33$	St	0.3	0.35	0.4	0.45	0.5
α_0						
45°		1st	1st	1st	1st	1st
40°		1st	1st	1st*	1st	2nd
35°		1st	1st	1st	1st	2nd
30°		1st	2nd	2nd	2nd	2nd
25°		2nd	2nd	2nd	2nd	2nd
20°		2nd	2nd	2nd	2nd	2nd
15°		2nd	2nd	2nd	2nd	2nd**

*Case 8 ; ** Case 35

Table 1.8: The maximum peak location of thrust coefficient C_T depending on the foil kinematics parameters

number (case 8) and the case of low angle of attack and high Strouhal number (case 35). When the foil moves toward the wall ($t/T = 0.25$), a strong vortex pair is observed in case 8 while the vortex pair seems weak in case 35. When the foil moves away from the wall ($t/T = 0.75$), as in case 8, the vortex pair shape is considerably different in comparison with when the foil moves toward to the wall. The vortex pair at $t/T = 0.75$ is formed horizontally, thus it may cause a decrease in the thrust force as shown in the 1.23(a). Meanwhile, in case 35, the shape of the vortex pair is relatively similar when the foil moves toward the wall. It makes the thrust force quite similar at the two peak instants. The formation of the vortex in the two cases shows the wall effect is stronger in the case of high angle of attack and low Strouhal number (case 8), and it leads the maximum peak location of thrust in the first-half phase of the 2-D numerical simulation. For the 3-D experiment, the different vortex formation at $t/T = 0.25$ and 0.75 is observed as same as 2-D simulation results, but the thrust coefficient profile is not much altered, as discussed in figure 1.14. The maximum thrust peak location in the second half-phase for the 3-D experiment is not a consequence of the wall effect.

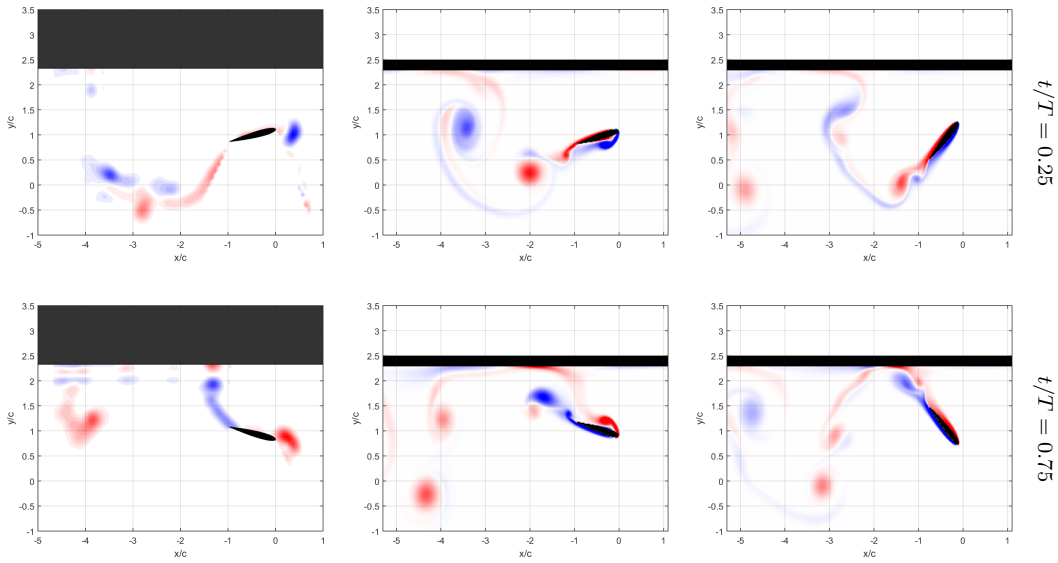

Figure 1.24: Vorticity plot of the 3-D experiment 2-D simulation at $t/T = 0.25$ and 0.75 in the case 8 ($St = 0.4$, $\alpha_0 = 40°$) and 35 ($St = 0.5$, $\alpha_0 = 15°$). The 3-D PIV image for case 35 is not available in this study.

1.6 Conclusions

We showed the inherent difference of the 2-D and 3-D dynamic wall effect by comparing images of vortex shedding of flapping foil motion with a 2-D numerical simulation and 3-D experiment results. Mivehchi et al. (2016) hypothesized this difference by analyzing the hydrodynamic forces. They conducted 3-D lab experiment, and approximated 2-D experiment using the small clearance at the tip of the foil. In this paper, the argument is enhanced by the comparison of vortex behaviors using 2-D experiments in numerical simulations and the Particle Image Velocimetry (PIV) from 3-D experiments. The following conclusions are observed in this paper:

1. The vortex pattern near the 3-D foil tip is significantly different from the vortex formation in the 2-D simulation. The span-wise flow from the tip causes the difference in vorticity plot along the foil; thus, alters the forces on the body.

2. Despite the wall effect on the flapping foil motion observed in both the 2-D simulation and 3-D PIV experiment, the vortex formation has discrepancies between 2-D and 3-D configuration. The vortex at the 3-D foil tip is enhanced by the wall existence and it leads to much difference in the force coefficient from the 2-D simulation.

3. The 2-D simulation has a unique behavior in thrust coefficient profile compared with the profile of the 3-D experiment in the case of low Strouhal numbers and high angle of attack, in which the wall effect is strong. It is possibly not appropriate to use the result of the 2-D simulation in this range to predict the thrust force characteristic.

The numerical simulation approach is highly useful to investigate the flapping foil motion and its ground effect, since it requires less expensive resources than those of lab experiments. To simplify the problems and reduce the cost, 2-D numerical solutions are often applied for analysis. However, to use the numerical solver appropriately, the understanding of the differences in the 2-D and 3-D phenomenon should be required.

List of References

Anderson, J., Streitlien, K., Barrett, D., and Triantafyllou, M. (1998). Oscillating foils of high propulsive efficiency. *Journal of Fluid Mechanics*, 360:41–72.

Chen, Y.-S. and Schweikhard, W. G. (1985). Dynamic ground effects on a two-dimensional flat plate. *Journal of Aircraft*, 22(7):638–640.

Cui, E. and Zhang, X. (2010). Ground effect aerodynamics. *Encyclopedia of Aerospace Engineering*.

De Silva, L. W. A. and Yamaguchi, H. (2012). Numerical study on active wave devouring propulsion. *Journal of marine science and technology*, 17(3):261–275.

Imamura, T., Suzuki, K., Nakamura, T., and Yoshida, M. (2005). Flow simulation around an airfoil by lattice boltzmann method on generalized coordinates. *AIAA journal*, 43(9):1968–1973.

Karbasian, H. R. and Esfahani, J. (2017). Enhancement of propulsive performance of flapping foil by fish-like motion pattern. *Computers & Fluids*, 156:305–316.

Liang, H., Wang, X., Zou, L., and Zong, Z. (2014). Numerical study of two-dimensional heaving airfoils in ground effect. *Journal of Fluids and Structures*, 48:188–202.

Licht, S., Wibawa, M., Hover, F., and Triantafyllou, M. (2010). In-line motion causes high thrust and efficiency in flapping foils that use power downstroke. *Journal of Experimental Biology*, 213(1):63–71.

Lockard, D. P., Luo, L.-S., Milder, S. D., and Singer, B. A. (2002). Evaluation of powerflow for aerodynamic applications. *Journal of Statistical Physics*, 107(1-2):423–478.

Maertens, A. P. and Weymouth, G. D. (2015). Accurate cartesian-grid simulations of near-body flows at intermediate reynolds numbers. *Computer Methods in Applied Mechanics and Engineering*, 283:106–129.

Mivehchi, A., Dahl, J., and Licht, S. (2016). Heaving and pitching oscillating foil propulsion in ground effect. *Journal of Fluids and Structures*, 63:174–187.

Molina, J. and Zhang, X. (2011). Aerodynamics of a heaving airfoil in ground effect. *AIAA journal*, 49(6):1168–1179.

Moriche, M., Flores, O., and García-Villalba, M. (2015). Generation of thrust and lift with airfoils in plunging and pitching motion. In *Journal of Physics: Conference Series*, volume 574, page 012163. IOP Publishing.

Pantula, S. R. (2008). *Modeling fluid structure interaction over a flexible fin attached to a NACA0012 airfoil*. Western Michigan University.

Perkins, M., Elles, D., Badlissi, G., Mivehchi, A., Dahl, J., and Licht, S. (2017). Rolling and pitching oscillating foil propulsion in ground effect. *Bioinspiration & biomimetics*, 13(1):016003.

Read, D. A., Hover, F., and Triantafyllou, M. (2003). Forces on oscillating foils for propulsion and maneuvering. *Journal of Fluids and Structures*, 17(1):163–183.

Wang, L. and Yeung, R. W. (2016). Investigation of full and partial ground effects on a flapping foil hovering above a finite-sized platform. *Physics of Fluids*, 28(7):071902.

Weymouth, G. D. (2015). Lily pad: Towards real-time interactive computational fluid dynamics. *arXiv preprint arXiv:1510.06886*.

Weymouth, G. D. and Yue, D. K. (2011). Boundary data immersion method for cartesian-grid simulations of fluid-body interaction problems. *Journal of Computational Physics*, 230(16):6233–6247.

Wu, J., Qiu, Y., Shu, C., and Zhao, N. (2014a). Pitching-motion-activated flapping foil near solid walls for power extraction: A numerical investigation. *Physics of Fluids*, 26(8):083601.

Wu, J., Shu, C., Zhao, N., and Yan, W. (2014b). Fluid dynamics of flapping insect wing in ground effect. *Journal of Bionic Engineering*, 11(1):52–60.

APPENDIX

Numerical Simulation Procedure

A.1 System Environment

The Lily Pad CFD code as updated on 3rd Jan 2017 is used in this thesis and obtained from Dr. Weymouths GitHub webpage (https://github.com/weymouth/lily-pad). This code is written and run in Processing (https://processing.org), an open source programming language based on Java, and it provides the flow visualization from the numerical solution calculated by the CFD code (Weymouth, 2015). The followings are the major code files written and used in the simulations. Some classes are modified for this study, thus the original class file in Lily Pad may not be compatible with this simulation code.

- `LilyPad.pde` : The main code for simulation
- `BDIM.pde` : The class to solve the Boundary Data Immersed Method equation for velocity and pressure
- `Body.pde` : The class to define the bodies in flow (modified)
- `NACA.pde` : The extension of Body class to create NACA foil body (modified)
- `BodyUnion.pde` : The class to unify the multiple bodies created
- `FloodPlot.pde` : The class for flow visualization.
- Other classes is not modified and same with those in original Lily Pad code package.

All simulations in this study are run in Microsoft Windows 7 system. To execute the simulations readily, the simulation code is exported to an application

that can be run with an input file of test parameters. The application of each simulation case consists of the followings.

- `LilyPad.exe` : The executable file to start the simulation
- `data` : The folder including the input parameter file (See section A.2)
- `source` : The folder including source codes
- `lib` : The library folder

A.2 Experiment Set-up

A Matlab code (`simul_gen.m`) is programmed to generate the simulation set for the flapping foil motion near a wall. The code creates input files (`input_cp.txt`) for 245 cases including parameters; the mean heave distance from the wall (H^*), Strouhal number (St), and the amplitude of the angle of attack (α_0) as shown in table A.1.

$H^* = 1.33, 1.66, 2, 3, 4, 5, 6$		Strouhal Number (St)				
		0.3	0.35	0.4	0.45	0.5
Max. nominal angle of attack (α_0)	15°	Case 31	Case 32	Case 33	Case 34	Case 35
	20°	Case 26	Case 27	Case 28	Case 29	Case 30
	25°	Case 21	Case 22	Case 23	Case 24	Case 25
	30°	Case 16	Case 17	Case 18	Case 19	Case 20
	35°	Case 11	Case 12	Case 13	Case 14	Case 15
	40°	Case 6	Case 7	Case 8	Case 9	Case 10
	45°	Case 1	Case 2	Case 3	Case 4	Case 5

Table A.1: Test matrix and numbering for flapping foil simulation

Given the parameters, the amplitude of pitch angle is determined in the code by applying functions (`amplitude_error.m` ,`velocity_function.m`) which

are used in the previous experiment (Mivehchi et al., 2016). The calculated pitch angle amplitude is also provided in the input parameter files.

List of References

Mivehchi, A., Dahl, J., and Licht, S. (2016). Heaving and pitching oscillating foil propulsion in ground effect. *Journal of Fluids and Structures*, 63:174–187.

Weymouth, G. D. (2015). Lily pad: Towards real-time interactive computational fluid dynamics. *arXiv preprint arXiv:1510.06886*.

BIBLIOGRAPHY

Anderson, J., Streitlien, K., Barrett, D., and Triantafyllou, M., "Oscillating foils of high propulsive efficiency," *Journal of Fluid Mechanics*, vol. 360, pp. 41–72, 1998.

Chen, Y.-S. and Schweikhard, W. G., "Dynamic ground effects on a two-dimensional flat plate," *Journal of Aircraft*, vol. 22, no. 7, pp. 638–640, 1985.

Committee, C. F. D., ""guide: Guide for the verification and validation of computational fluid dynamics simulations (aiaa g-077-1998(2002))"," 2002.

Cui, E. and Zhang, X., "Ground effect aerodynamics," *Encyclopedia of Aerospace Engineering*, 2010.

De Silva, L. W. A. and Yamaguchi, H., "Numerical study on active wave devouring propulsion," *Journal of marine science and technology*, vol. 17, no. 3, pp. 261–275, 2012.

Imamura, T., Suzuki, K., Nakamura, T., and Yoshida, M., "Flow simulation around an airfoil by lattice boltzmann method on generalized coordinates," *AIAA journal*, vol. 43, no. 9, pp. 1968–1973, 2005.

Karbasian, H. R. and Esfahani, J., "Enhancement of propulsive performance of flapping foil by fish-like motion pattern," *Computers & Fluids*, vol. 156, pp. 305–316, 2017.

Liang, H., Wang, X., Zou, L., and Zong, Z., "Numerical study of two-dimensional heaving airfoils in ground effect," *Journal of Fluids and Structures*, vol. 48, pp. 188–202, 2014.

Licht, S., Wibawa, M., Hover, F., and Triantafyllou, M., "In-line motion causes high thrust and efficiency in flapping foils that use power downstroke," *Journal of Experimental Biology*, vol. 213, no. 1, pp. 63–71, 2010.

Lockard, D. P., Luo, L.-S., Milder, S. D., and Singer, B. A., "Evaluation of powerflow for aerodynamic applications," *Journal of Statistical Physics*, vol. 107, no. 1-2, pp. 423–478, 2002.

Maertens, A. P. and Weymouth, G. D., "Accurate cartesian-grid simulations of near-body flows at intermediate reynolds numbers," *Computer Methods in Applied Mechanics and Engineering*, vol. 283, pp. 106–129, 2015.

Mivehchi, A., Dahl, J., and Licht, S., "Heaving and pitching oscillating foil propulsion in ground effect," *Journal of Fluids and Structures*, vol. 63, pp. 174–187, 2016.

Molina, J. and Zhang, X., "Aerodynamics of a heaving airfoil in ground effect," *AIAA journal*, vol. 49, no. 6, pp. 1168–1179, 2011.

Moriche, M., Flores, O., and García-Villalba, M., "Generation of thrust and lift with airfoils in plunging and pitching motion," in *Journal of Physics: Conference Series*, vol. 574, no. 1. IOP Publishing, 2015, p. 012163.

Pantula, S. R., *Modeling fluid structure interaction over a flexible fin attached to a NACA0012 airfoil*. Western Michigan University, 2008.

Perkins, M., Elles, D., Badlissi, G., Mivehchi, A., Dahl, J., and Licht, S., "Rolling and pitching oscillating foil propulsion in ground effect," *Bioinspiration & biomimetics*, vol. 13, no. 1, p. 016003, 2017.

Read, D. A., Hover, F., and Triantafyllou, M., "Forces on oscillating foils for propulsion and maneuvering," *Journal of Fluids and Structures*, vol. 17, no. 1, pp. 163–183, 2003.

Wang, L. and Yeung, R. W., "Investigation of full and partial ground effects on a flapping foil hovering above a finite-sized platform," *Physics of Fluids*, vol. 28, no. 7, p. 071902, 2016.

Weymouth, G. D., "Lily pad: Towards real-time interactive computational fluid dynamics," *arXiv preprint arXiv:1510.06886*, 2015.

Weymouth, G. D. and Yue, D. K., "Boundary data immersion method for cartesian-grid simulations of fluid-body interaction problems," *Journal of Computational Physics*, vol. 230, no. 16, pp. 6233–6247, 2011.

Wu, J., Qiu, Y., Shu, C., and Zhao, N., "Pitching-motion-activated flapping foil near solid walls for power extraction: A numerical investigation," *Physics of Fluids*, vol. 26, no. 8, p. 083601, 2014.

Wu, J., Shu, C., Zhao, N., and Yan, W., "Fluid dynamics of flapping insect wing in ground effect," *Journal of Bionic Engineering*, vol. 11, no. 1, pp. 52–60, 2014.